Available online at www.sciencedirect.com

ScienceDirect

Energy Procedia 148 (2018) 703–711

Energy Procedia

www.elsevier.com/locate/procedia

73rd Conference of the Italian Thermal Machines Engineering Association (ATI 2018), 12–14 September 2018, Pisa, Italy

CFD analysis of a swirl stabilized coal combustion burner

G.D. Rago[1], G. Rossiello[3], R. Dadduzio[3], T. Giani[2], A. Saponaro[3], F. Cesareo[1], M. Lacerenza[1], F. Fornarelli[1], G. Caramia[1], B. Fortunato[1], S.M. Camporeale[1], M. Torresi[1], V. Panebianco[3]*

[1]*Politecnico di Bari – DMMM – Via Re David, 200 – 70125 Bari (BA) - Italy*
[2]*AC Boilers S.p.A. – Largo Buffoni n°3 – 21013 Gallarate (VA) – Italy*
[3]*CCA - Via Milano km 1,600 - 70023, Gioia Del Colle (BA), Italy*

Abstract

Anthropogenic Greenhouse Gases (GHG) emissions have increased since the pre-industrial era, driven by the economic and population growth. In the last decades, significant efforts have been made to develop cleaner and more efficient technologies able to control GHG emissions. In the field of combustion burners, this commitment strongly relies on the development of new and detailed numerical models, which allow a deep investigation of complex burner performance and a significant reduction of full-scale experimental costs. The knowledge previously acquired on the TEA-C coal burner CFD study is here expanded in the framework of the Be4GreenS project, targeting to the development of a new generation of burners. The new implemented model accounts for the detailed chemical and kinetic characterization of the pulverized coal together with the exact inner volume geometry of the experimental combustion chamber and the actual extension of the heat exchanging and refractory surfaces. In addition, the secondary and tertiary air registers are here numerically investigated. The outcome from the CFD analysis is validated against the experimental data. The NOx formation analysis is also provided.

Keywords: CFD; Turbulent combustion, Pulverized coal; Low-NOx burner

* Corresponding author.
E-mail address: vincenzo.panebianco@acboilers.com

10.1016/j.egypro.2018.08.160

1. Introduction

The transition from an intense fossil fuel consumption to the broad diffusion of renewable energies, involves an intermediate phase where more efficient technologies are developed in order to improve current power generation technologies. The current rate of transition, however, is far from being sufficient to reach the challenging targets set in 2015 during the 21st Session of the Conference of Parties (COP21), where the 196 attending parties agreed to reduce their carbon output in order to keep the global warming below 2°C, a value generally accepted as a threshold beyond which climate change becomes potentially catastrophic [1].

The proposed GHG mitigation pathway requires a substantial emissions reduction (from 40 to 70% lower than 2010) over the next few decades and near zero emissions of cumulating GHG by the end of the 21st century [2]. This scenario strongly relies on the wide implementation of carbon capture systems and highly efficient low-NOx combustion technologies such as aerodynamically staged burners. MILD combustion with solar air preheating [4] has also caught the attention of scientific and industrial community because of its promising features of both high efficiency and lower pollutant emissions. The investment patterns will behave similarly, experiencing large changes in the near future. Over the next two decades, annual investments in conventional fossil fuel technologies associated with the electricity production are projected to decline, while annual investment in low carbon electricity supply will significantly rise [2].

These technical goals cannot be reached without a deep understanding of the turbulence-flame interaction in furnace operation. In this regard, CFD analysis is universally recognized by the combustion community as a powerful and valuable tool to gain insights into industrial flame behavior.

Starting from 2008 a technical partnership between the Polytechnic University of Bari, AC Boilers and CCA has been set-up in order to develop high quality pulverized coal combustion CFD models, achieving good agreement between experimental and numerical data [2], [3]. Because of the typically small dimension of turbulent scales in highly turbulent flows and the complexity of the aerodynamically staged coal burners geometry, a high degree of accuracy was possible in the past only with the upfront cost of highly demanding computational resources. For this reason some level of simplifications were introduced in the 2010 to reduce the numerical effort.

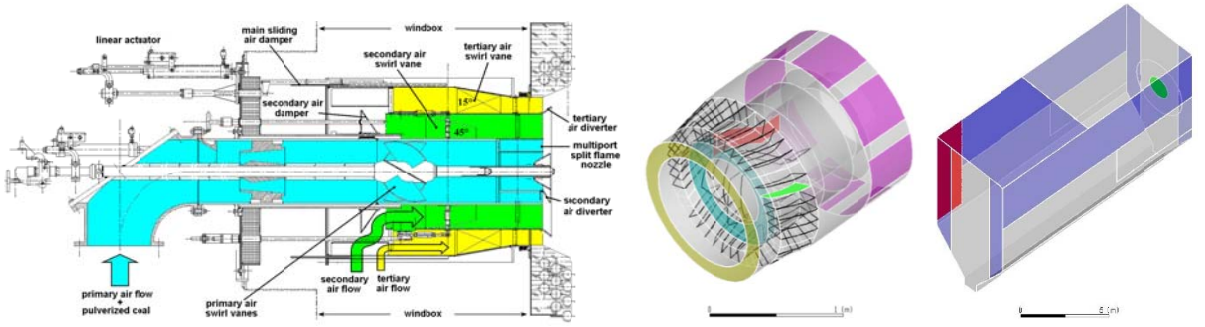

Fig. 1 The figure shows in order: a) primary air duct and air registers cross section area; b) wind-box numerical domain (the air inlets are highlighted in purple, secondary-outlet in cyan, tertiary outlet in yellow, a secondary-swirler-blade in red, and a tertiary-swirler-blade in green); c) combustion chamber numerical domain (the exhaust gas outlet is highlighted in red, the heat exchanging areas in blue and the remaining refractory walls in grey).

Following the recent progress in High Performance Computing (HPC), an increased level of complexity of the domain studied is today allowed. As such, chance for improving the experimental/numerical data match was found by rising the 2010 model level of details. The major changes regard the application of coal specific data for the devolatilization and the char burnout models, as well as the application of the Discrete Ordinate (DO) radiation model. In particular, the fuel properties were provided by the CNR "National Research Center" of Naples following a detailed coal characterization. This avoided any assumption of the coal chemical characteristics based on the literature data. It should be noted that, despite both extracted from South-African mines, the sample investigated by CNR and the one actually used to fuel TEA-C burner slightly differ from each other (Tab.2).

A schematic of the TEA-C burner is shown in figure 1. The TEA-C geometry is characterized by three air registers designed to stage the fuel/oxidizer chemical interaction. The primary air transports the pulverized coal from the coal mill to a multi-port split flame nozzle. The secondary swirled air encloses the primary flow hampering its radial spreading. Tertiary swirled air is then staged for combustion completion purposes. Both secondary and tertiary air flows are swirled clockwise (45° and 15°, respectively).

Along with the fully characterized coal model, an important improvement with respect to the previous study regards the modelling of the secondary and tertiary air registers and their addition in the computational domain. As such, assumptions on the secondary and tertiary air flow patterns entering the combustion chamber are also avoided. The computational domain also considers the exact inner volume of the combustion chamber geometry along with the actual extension of the heat exchanging and refractory surfaces. Renderings of the primary air duct, the air registers and combustion chamber are shown in Fig. 1.

In order to have a clear picture of the NOx formation within the burner, a simplified chemical kinetics is used with a post-processing approach: a reduced number of global reactions are considered coupled with the velocity, temperature and species concentration fields a priori computed.

2. TEA-C CFD model

The computational domain has been discretized by means of a hybrid multi-block mesh (about 16.5 million of cells). According to 2008 experimental tests, the boundary/inlet conditions have been set as follows: coal particle mass flow rate, G_{PV} = 1.276 at T_{PV} = 356 K (LHV_{DAF} = 32M J/kg for a total thermal input of 34.2 MW); primary air mass flow inlet, $G_{a,1}$ = 2.64 kg/s at T_1 = 356K; windbox air mass flow rate, G_{wb} = 10 kg/s at T_{wb} = 564 K (resulting in a combustion excess air of 15%). Concerning the heat transfer boundary conditions, different materials are employed throughout the combustion chamber surfaces modeled with an overall heat transfer coefficient ranging from 3.8 to 28.3 W/(m^{2}K) and internal emissivity 0.4, whereas the overall heat transfer coefficient is 5000 W/(m^{2}K) for evaporator walls, considering a 485 K free stream temperature and a 0.5 internal emissivity.

The continuous phase flow is computed by solving the Reynolds Averaged Navier Stokes (RANS) equations, with a 2-equations realizable k-ε model for turbulence closure, discretized according to a finite volume approach. Non equilibrium wall functions have been used for the near-wall treatment of turbulence.

Combustion in continuous phase has been modeled by the non-premixed combustion approach employing a single fuel stream and an oxidizer stream with a single mixture fraction Z describing the mixture composition and a probability density function (PDF) to take into account reactions and turbulence-chemistry interaction. PDF look-up tables have been computed for a fifty-species mixture, from which, given the enthalpy, the mixture-fraction and its variance, all the gas-mixture thermodynamic and transport properties (density, constant pressure specific heat capacity, molecular viscosity) can be evaluated. Sutherland's viscosity law has been considered in order to deal with the molecular viscosity dependency on temperature, while for the continuous phase density an ideal gas state equation has been assumed such that it depends on temperature while it is independent of the local pressure (incompressible model with constant bulk pressure).

The pulverized coal has been treated as a discrete phase and modeled by means of a two-way coupling Lagrangian approach. The collisions of the coal particles with the burner walls and internals have been treated as elastic while an inelastic (no-bounce) condition has been assumed for collisions with the combustion chamber walls. The particle distribution at the domain inlet and the coal characteristics are based on the pulverized coal actually used in the experimental test. The pulverized coal was milled and then classified by means of a rotating sieve at 200 rpm (99.90% with d < 300 μm, 99.45%with d < 150 μm, 90.00% with d < 75 μm), obtaining a diameter distribution well approximated by a Rosin–Rammler distribution with the following parameters: minimum diameter of 5 μm, maximum diameter of 300 μm, mean diameter of 40 μm and spread parameter of 1.31. The discrete solid phase enters the domain by a uniformly distributed *injection* from the primary air inlet, divided into 268'800 *parcels* obtained as *the number of faces* (5376) multiplied by the *number of diameters* considered in the Rosin-Rammler distribution (10) multiplied by the *number of turbulent tries* (5) for each stream.

Radiative heat transfer has been accounted for by means of the DO (Discrete Ordinate) model, solving the Radiation Transfer Equation with a Finite Volume discretization on a discrete number of directions. A domain-based Weighted-Sum-of-Gray-Gases Model (WSGGM) approach has been used to derive the absorption coefficient in the

continuous phase. Particle-gas radiation interaction has been taken into account, assuming particle emissivity of 0.9 and scattering coefficient equal to 0.6 [4].

The pulverized coal combustion process has been subdivided into the following steps: (i) inert heating; (ii) devolatilization; (iii) volatile matter combustion (homogeneous combustion in the continuous phase); (iv) char burnout (heterogeneous combustion on the particle surface releasing CO_2 in the gas phase). The inert heating laws are applied when the particle temperature is lower than the assigned devolatilization temperature. The devolatilization law is applied when the temperature of the particle reaches a temperature of 623 K, until the mass of the particle, exceeds the mass of the non-volatiles in the particle. The moisture content of coal particles and the particle swelling during the devolatilization process have been neglected.

The *Chemical Percolation Devolatilization* (CPD) model has been employed to describe the devolatilization process under rapid heating conditions. It considers the thermo-chemical transformations of the coal structure rather than using empirical relationships [10]. As such, input data required by the CPD model (5) are coal-specific, obtainable by means of solid-state ^{13}C Nuclear Magnetic Resonance (NMR) spectroscopy. The CPD parameters (see Table 1) have been supplied by the CNR of Naples, as a result of NMR analysis on a South African coal very similar to the Kleinkopje's coal, burned during the experimental tests at CCA. For the sake of completeness, the proximate and ultimate analyses are reported in Table 2. The thermal annealing effect was taken into account reducing the Kinetic-Limited Rate Pre-Exponential value by a factor 10. Char porosity has been also experimentally evaluated by CNR.

Table 1 – Coal-specific CPD parameters for KleinKopje and South African coal (CNR analysis)

Parameter	Symbol	Kleinkopje	SA coal	Unit
Initial fraction of bridges in the coal lattice	p_0	0.83	0.667	-
Initial fraction of char bridges	C_0	0	0.003	-
Lattice coordination number	$\sigma+1$	5.2	5.17	-
Cluster Molecular Weight	MW_1	308	302.2	kg/kmole
Side Chain Molecular Weight	MW_δ	30	30.1	kg/kmole

Table 2 – Proximate and Ultimate analysis for KleinKopje and South African coal (CNR analysis)

	Proximate Analysis (weight % dry basis)			Ultimate Analysis (weight % dry ash free basis)				
	Ash	Volatile	Char	C	H	O	N	S
Kleinkopje	13.97	24.46	61.57	83.77	4.49	9.31	1.89	0.53
SA coal	15.66	23.13	61.21	80.63	4.51	12.69	1.42	0.76

Table 3 – Kinetic/diffusion limited surface reaction rate parameters for KleinKopje and South African coal (CNR analysis)

Parameter	Symbol	Kleinkopje	SA coal	Unit
Mass Diffusion-Limited Rate Constant	C_1	$5 \cdot 10^{-12}$	$5 \cdot 10^{-12}$	-
Kinetic-Limited Rate Pre-Exponential Factor	A_i	0.0302	0.00011	-
Kinetic-Limited Rate Activation Energy	E_i	$1.794 \cdot 10^{8}$	$1.2 \cdot 10^{8}$	Joule/kmole
Char Porosity	θ	0.67	0.18	-
Mean Pore Radius	r_p	$6 \cdot 10^{-8}$	$6 \cdot 10^{-7}$	m
Specific Internal Surface Area	A_g	300'000	300'000	m^2/kg
Tortuosity	τ	1.4142	2	-
Burning Mode	α	0.25	0.25	-

Char burnout process has been modeled by means of the Intrinsic Model that computes the heterogeneous reaction rate considering both kinetics and diffusion phenomena. The major Intrinsic model parameters are summarized in Tables 3, where both KleinKopje coal data [7] and South African coal data (from CNR) are compared.

In order to predict NOx emissions, a transport equation for nitric oxide (NO) concentrations has been solved. The NOx formation has been evaluated according to the thermal and fuel-NO mechanisms; hence, two additional transport equations for intermediate species (HCN and NH_3) have been considered. The NOx transport equations are solved in post-processing based on frozen flow fields and combustion solutions.

The formation of thermal NOx is determined according to the extended Zeldovich mechanism, and the rate constants have been selected based on the evaluation of Hanson and Salimian [12]. The needed concentrations of O, H and OH are derived by temperature and O_2 and H_2O concentrations by means of an heuristic relation.

Organic compounds present in coal and containing nitrogen can significantly contribute to the total NOx formed during the combustion process. Fuel nitrogen is split between volatiles and char during coal devolatilization and in the nitrogen conversion can originate hydrogen cyanide (HCN) and/or ammonia (NH_3). Local NH_3 and HCN concentrations derive from the solution of the respective transport equations solved in post-processing according to the kinetics developed by De Soete [13]. With bituminous coal, better NOx predictions are obtained when using an HCN/NH_3 partition ratio of 9:1. The nitrogen contained in the char is then heterogeneously oxidized to NO via an overall reaction.

3. 2018 TEAC Numerical Study – CFD results.

The three air fluxes enter the combustion chamber with different velocity magnitudes (Primary Air (PA): ~ 35m/s; Secondary Air (SA): ~ 40m/s; Tertiary Air (TA): ~ 33m/s).

Those values have been computed as mass weighted averages along the TA, SA and each coal nozzle surface. The SA/TA air split is 0.7, which correspond to partition fractions of SA=41% and TA=59%. The secondary and tertiary air registers swirl the SA and TA flows with angles equal to 45° and 15° degree respectively.

The temperature contour along the YZ plane, Fig. 2, shows an average temperature of approximately 1500K within the combustion chamber and a temperature of approximately 1700K in the near-burner region.

The flame core presents a not completely symmetrical structure with respect to the burner axis. The turbulent flow observed within the burner is clearly unsteady, with effects accentuated by the swirl and by the presence of bluff bodies, which create recirculating and high vorticity zones. At numerical and simulation levels, this aspect is highlighted by the pseudo-periodic behavior of both local and integral variables. However, this unsteadiness is limited (<5%) and lower than the commonly accepted approximation for this type of investigation and therefore do not affect the results obtained. Moreover, in regard to the asymmetries, which are correctly captured as highlighted in the figures contained in the article, these are substantially attributable to the following effects (in order of relevance): 1) non symmetrical injection of the pulverized coal into the combustion chamber (see Fig. 3) geometric asymmetry of the combustion chamber with gas outlet on one side; 3) heat exchange asymmetry in the combustion chamber, due to the non-symmetrical distribution of evaporating tubes and refractory surfaces. The coal particle tracks along the same plane show a similar trend, shedding light on a non-uniform coal distribution in the CC. This trend is explained by the coal distribution along the burner. Downstream the nozzles it is possible to observe a higher particle concentration in the lower openings with respect to the upper ones. A non-uniform coal concentration is also observed downstream each coal nozzle: this is due to a high coal concentration in the upper part of the primary duct, which the swirler homogenizes only partially.

The velocity vectors in Fig. 2 highlight more recirculation zones within the combustion chamber. This was expected since the fully turbulent nature of the flows under investigation. Particularly interesting is the small recirculation zone identifiable in the near burner zone, where a significant coal particle recirculation is desirable in order to reduce the NO_x. The fully turbulent flow behavior is reflected by the paths followed by the coal, which show a significant recirculation area, particularly in the far end of the combustion chamber. The averaged particle residence time results to be about 4 s, with about 2 s needed to reach the near burner area from the burner inlet.

In Fig. 5, the most interesting variables are shown as contour plots on the YZ plane and on 3 cross-sections passing through three experimental windows (W2, W3 and W5, for which measured quantities are available). Two

black solid lines are overlaid on each contour, namely IRZ and Z_{st}. The IRZ line marks the outer surface of the Internal Recirculation Zone, defined as the area where the axial components of the velocity vectors are negative. Within this area a significant recirculation of the primary air back to the near burner zone is observed. The second black line on the other hand, represents the stoichiometric mixture fraction region, hereafter referred as Z_{st} (here Z_{st} = 0.08896). The mixture fraction is a common tool used to investigate reactant mixing under non-premixed conditions and provides insights into the local fuel/oxidizer ratio. Z is a passive (or conserved) scalar which changes its value because of diffusion and convection, but not for reaction, since elements are conserved during combustion. The line encloses the area where $Z > Z_{st}$, highlighting a fuel rich region.

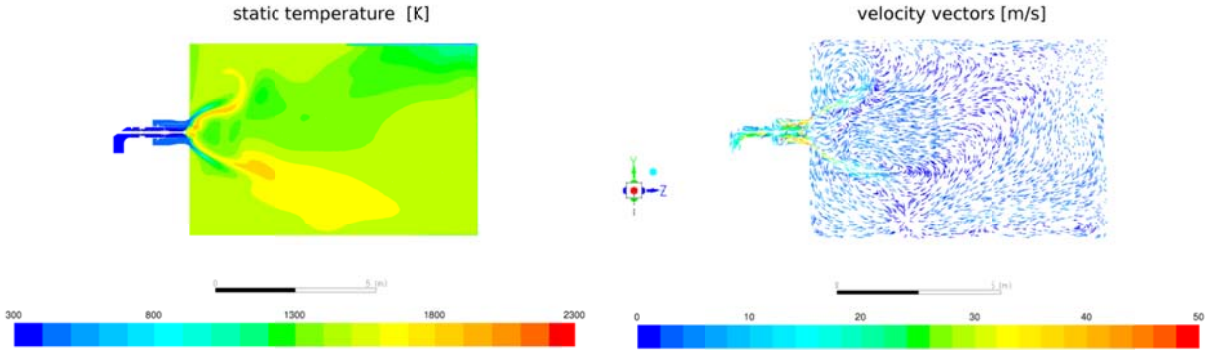

Fig. 2 Contour of static temperature (left) and velocity vectors coloured by velocity magnitude (right), both on the YZ plane.

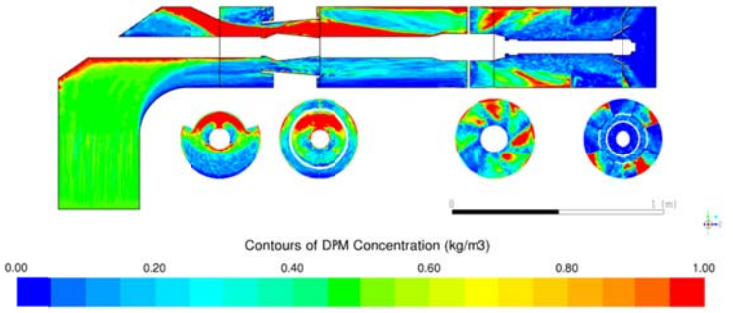

Fig. 3 Contour of DPM Concentration (kg/m^3) on primary duct, with distribution highlighted on four different transversal sections.

The flame core presents a non-symmetrical behavior along the YZ plane section. The flame spreads radially, because of the swirled motion, as it move along the axial direction (contours along XY planes). The Z_{st} line nicely fit the hottest part of the flame up to the W5. Within this volume, the stoichiometric iso-line encloses the vast majority of reactants and products, correctly delimiting the fuel rich region. At the fuel-rich/oxidizer interface the highest temperature are observed.

The oxygen depletion is clearly visible within Z_{st}. High O_2 levels are observed in the near burner volume, immediately outside the Z_{st} iso-line. Here, significant volatile release and char burnout rates are spotted. In particular the devolatilization process is almost complete at W2 while the contours of char burnout show that this process goes further downstream up to W5.

Both devolatilization and char burnout processes are particularly intense along the planes crossing the coal nozzles, where pulverized coal meets secondary and tertiary air flows. Going into more details, the volatile release is caught outside the IRZ, immediately after the cone. Here high temperature and high level of oxygen are present. The similarity of NO and O2 flow patterns suggests a strong linkage between oxygen level and nitrogen oxide emissions. Significant NO presence is observed at the fuel-rich/oxidizer interface, just outside the Z_{st}.

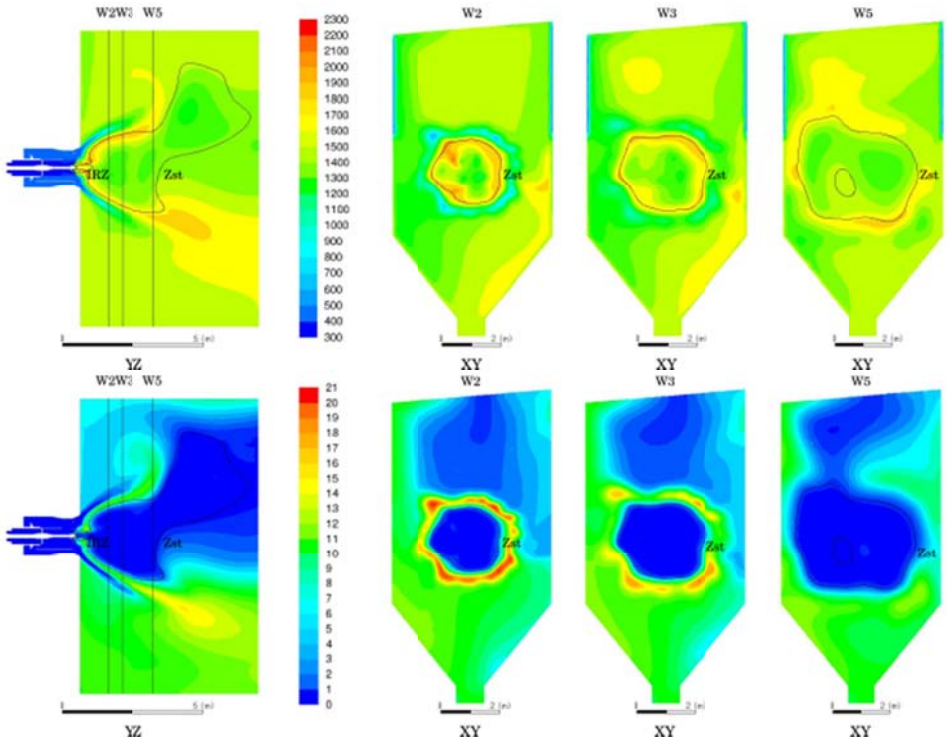

Fig. 4 Contours on YZ plane and 3 cross-sections in the near-burner region of: Temperature (1st row), O_2 mass fraction (2rd).

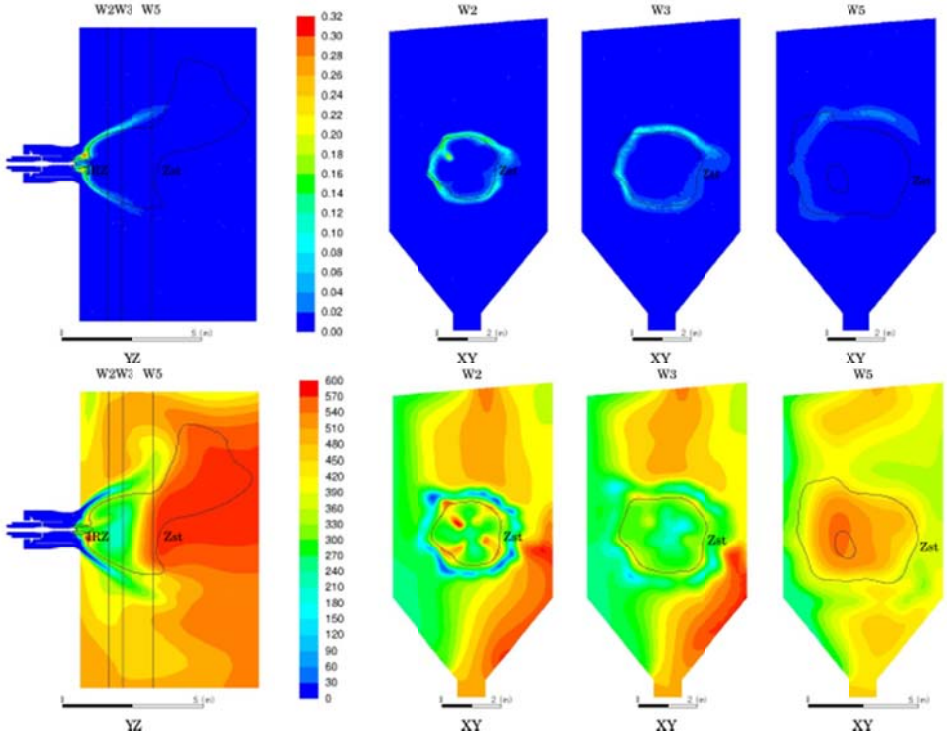

Fig. 5 Contours on YZ plane and 3 cross-sections in the near-burner region of: Char Burnout (1st row) and NO ppm dry (2rd).

4. Numerical model validation

The TEA-C numerical model has been validated against experimental data gathered along three different traversing close to the burner head (marked as W2, W3 and W5). In addition, numerical data from the CC outflow surface are compared with experimental data recorded during the 2008 test campaign. Values recorded at the outflow are integrated along the CC surface and mass-weighted averaged with the only exception of the flue gas temperature values, which are recorded at the Middle (M) and Bottom (B) point of the CC exit only. The values of Temperature, CO_2, O_2, NO, SO_2 and UBC (Unburnt Carbon) are compared in Fig. 6. It is worth noting that UBC values numerically evaluated are referred to the coal mass flow rate (dry) injected at the burner inlet. It follows that the experimental UBC measure (Carbon left in ashes) is evaluated according to a different procedure.

The good match between experimental and numerical data highlights the quality of the developed model. Better predictions are observed along W2 and W3 while a more significant data mismatch is spotted along W5. The flame core width is correctly estimated, as demonstrated by the Temperature and O2 profiles peaks showing a fairly good agreement with the experimental data. Also the NO profiles, usually difficult to be predicted, show a good agreement with the experimental data, especially in proximity of the burner axis (-1 m < X < 1 m).

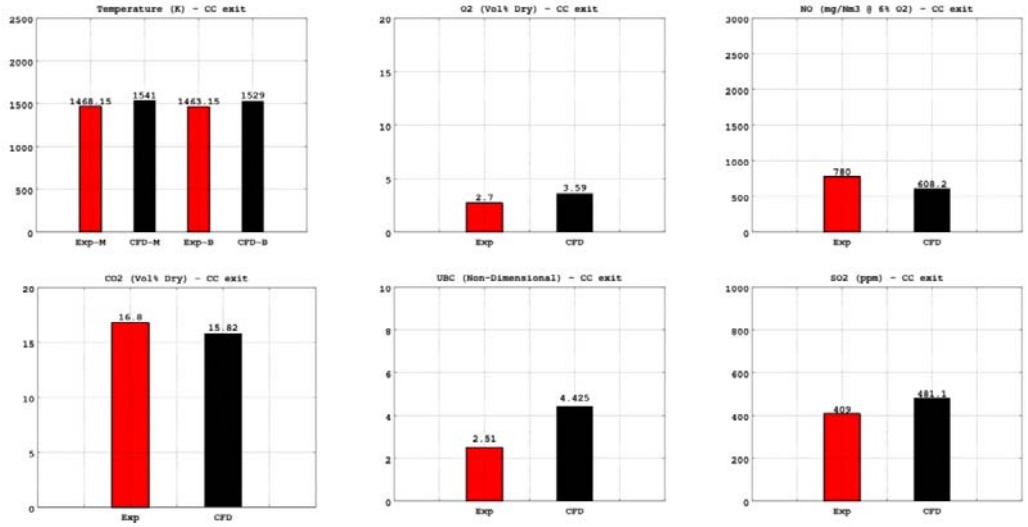

Fig. 6 CFD results vs experimental data: exit temperature (M=middle probe, B=bottom probe), O_2 and NO (first row) and CO_2, UBC, SO_2 (second row) recorded at the combustion chamber exit surface.

5. Conclusions

In this work, the previously investigated TEA-C burner is reconsidered in the light of some improvements both in the CFD modeling and in the definition of the computational domain. Actually, the exact inner volume geometry of the experimental combustion chamber has been taken into account along with the actual extension of the heat exchanging and refractory surfaces. Finally, the windbox, feeding secondary and tertiary air, has been integrated in the computational domain. The major changes have regarded the application of coal specific data for both the devolatilization and the char burnout models, which have been computed from coal data being experimentally calculated by the CNR of Naples rather than estimated based on data retrieved in the literature. The radiation model was changed using the DO radiation model. The outcome from the CFD analysis has been validated against experimental data. Thermal, fuel and prompt NOx formation analysis has also been provided.

Acknowledgements

This work has been carried out in the Be4GreenS project (WDJBJ73) financed by the Apulia Region (PO FESR

2014/2020 -Titulus II - “Contribution to the investment programs of the big enterprises” – Act n. 799 del 07.05.2015

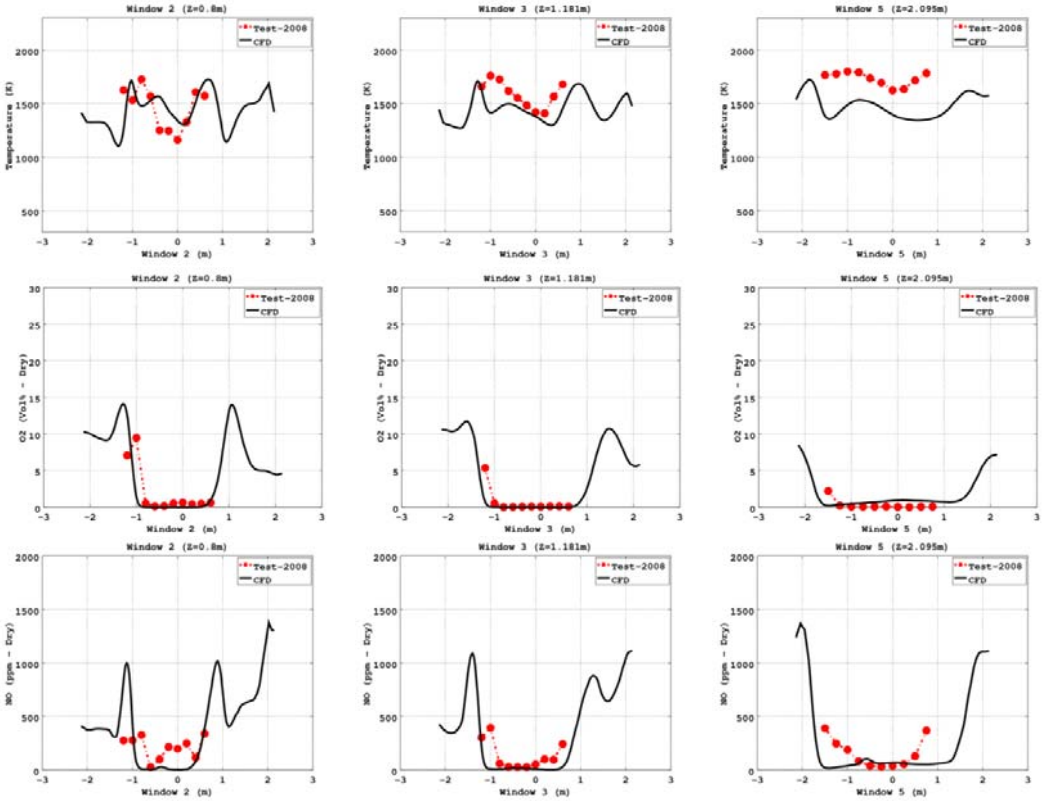

Fig. 7 CFD vs experimental data: Temperature (first row), O_2 (second row) and NO (third row) profiles along W2, W3 and W5.

References

[1] Intergovernmental Panel on Climate Change 2015. Climate Change 2014 – Mitigation of Climate Change. ISBN 978-92-9169-142-5.

[2] Hansen J, Kharecha P, Sato M, Masson-Delmotte V, Ackerman F, Beerling DJ, Hearty PJ, Hoegh-Guldberg O, Hsu SL, Parmesan C, Rockstrom EJ, Sachs J, […], Zachos JC, (2013). Assessing “Dangerous Climate Change”: Required Reduction of Carbon Emissions to Protect Young People, Future Generations and Nature. PLOS ONE 8(12).

[3] Torresi M, Panebianco V, Fortunato B, Camporeale SM, Saponaro A (2010). CFD analysis of a pulverized coal combustion burner. In: Proceedings of the 65th ATI National Congress. Domus de Maria (CA), 13-17 Settembre 2010.

[4] Milanese M, Torresi M, Colangelo G, Saponaro A, de Risi, A (2018). Numerical Analysis of a Solar Air Preheating Coal Combustion System for Power Generation, Journal of Energy Engineering, 144 (4), art. no. 04018038.

[5] Ranade VV, Gupta DF, (2015). Computational Modeling of Pulverized Coal Fired Boiler, CRC Pres, ISBN: 13: 978-1-4822-1535-9

[6] Torresi M, Fornarelli F, Fortunato B, Camporeale SM, and Saponaro A, (2017). Assessment against Experiments of Devolatilization and Char Burnout Models for the Simulation of an Aerodynamically Staged Swirled Low-NOx Pulverized Coal Burner. Energies 66(10).

[7] Torresi M, Fortunato B, Camporeale SM, and Saponaro A, (2012). A CFD modeling of pulverized coal combustion in an industrial burner. In Proceedings of the ASME Turbo Expo, Copenhagen, Denmark, 11–15 June 2012.

[8] Bireswar P, and Datta A, (2008). Burner development for the reduction of NOx emissions from coal fired electric utilities. Recent Pat. Mech. Eng. 1: 175–189, doi: 10.2174/2212797610801030175.

[9] FLUENT: User’s Guide 6.3; Fluent Inc.: Lebanon, NH, USA, (2006).

[10] Fletcher TH, Kerstein AR, Pugmire RJ, Solum MS, and Grant DM, (1992). Chemical percolation model for devolatilization. Direct use of 13C NMR data to predict effects of coal type. Energy Fuels 6(4): 414–431, doi: 10.1021/ef00034a011.

[11] Haas J, Masato T, Weber MR, (2001). Characterization of coal blends for pulverized coal combustion. Fuel 80(9): 1317–1323, doi: 10.1016/S0016-2361(00)00216-7.

[12] Hanson RK and Siamak S, (1984). Survey of Rate Constants in the N/H/O System. In: Gardiner W.C. (eds) Combustion Chemistry. Springer, New York, NY. Online ISBN 978-1-4684-0186-8.

[13] De Soete GG, (1975). Overall Reaction Rates of NO and N2 Formation from Fuel Nitrogen. In Proceedings of the 15th International Symposium on Combustion, Tokyo, Japan, 25–31 August 1975; pp. 1093–1102.